α-decaying states ^{18}O, ^{20}Ne and ^{22}Ne in ^{18}O beam induced reactions

S. Yildiz,[1] M. Freer,[1,*] N. Soić,[2] S. Ahmed,[1] N. I. Ashwood,[1] N. M. Clarke,[1] N. Curtis,[1] B. R. Fulton,[3] C. J. Metelko,[1,†] B. Novatski,[4] N. A. Orr,[5] R. Pitkin,[3] S. Sakuta,[4] and V. A. Ziman[1]

[1]*School of Physics and Astronomy, University of Birmingham, Edgbaston, Birmingham B15 2TT, United Kingdom*

[2]*Rudjer Bosković Institute, Department of Experimental Physics, Bijenicka 54, HR-10000 Zagreb, Croatia*

[3]*Department of Physics, University of York, Heslington, York YO10 5DD, United Kingdom*

[4]*RRC Kurchatov Institute, Kurchatov sq. 1, RU-123182 Moscow, Russia*

[5]*Laboratoire de Physique Corpusculaire, ENSICAEN et Université de Caen, IN2P3-CNRS, F-14050 Caen Cedex, France*

(Received 26 October 2005; published 6 March 2006)

The three reactions ^{12}C(^{18}O,^{14}C + α)^{12}C, ^{12}C(^{18}O,^{16}O + α)^{10}Be, and ^{12}C(^{18}O,^{18}O + α)^{8}Be have been used to investigate α-decaying states in the nuclei ^{18}O, ^{20}Ne, and ^{22}Ne populated through inelastic scattering, 2p, and α transfer, respectively. The measurements were performed at a beam energy of 140 MeV, and two charged particle detector telescopes were used to detect the breakup of the projectile-like particle. States in ^{18}O, ^{20}Ne, and ^{22}Ne were observed in the excitation energy range from 7 to 22 MeV and angular correlation techniques were used to determine the spins of a number of these states. The data are interpreted in terms of the underlying cluster structure. In the case of the ^{18}O, ^{14}C core + α, cluster bands, that are the analog of those in ^{20}Ne have been identified.

DOI: 10.1103/PhysRevC.73.034601 PACS number(s): 27.20.+n, 27.30.+t, 23.60.+e

I. INTRODUCTION

The ^{16}O + α cluster structure of the nucleus ^{20}Ne has often been cited as the best example of clustering in light nuclei (e.g., Ref. [1]). From the experimental perspective the level structure of ^{20}Ne has been characterized in terms of bands with both ^{16}O + α and [2,3]^{12}C + ^{8}Be [4] cluster configurations up to energies above 20 MeV. These states have been characterized in terms of their reduced widths, which demonstrate that in many of the bands the cluster structure is the dominant component [2]. The α + ^{16}O cluster structure of the ground state is intrinsically mass asymmetric, which gives rise to an octupole parity doublet of $K^{\pi} = 0^{\pm}$ bands [5,6]. The energy splitting between the two components has been interpreted in terms of the probability for the α particle to tunnel between the two sides of the ^{16}O core. The cluster structure of ^{20}Ne is also well reproduced within the antisymmetrized molecular dynamics (AMD) framework [7], a prescription that, importantly, is essentially free from any constraints on the arrangement of the 20 nucleons (i.e., a priori no clustering).

The impact of this remarkable structure on neighboring nuclei is important. For example, the ^{16}O + α cluster structure has been found to strongly influence the structure of ^{21}Ne [8], which demonstrates the molecular exchange of the valence neutron between the mass asymmetric cores. Furthermore, ^{18}O + α resonance scattering studies [9,10] have uncovered evidence for a sequence of resonances in ^{22}Ne that were interpreted in terms of the molecular exchange of two neutrons between the cores. The removal of two protons from ^{20}Ne forms ^{18}O, a nucleus that has also been demonstrated to display a mass-asymmetric character [11–13]. The precise link between the cluster structures in these nuclei remains, however, to be elucidated.

In the present paper we present measurements of the α decay of states in ^{18}O, ^{20}Ne, and ^{22}Ne measured simultaneously. These data provide a means to link the cluster structures in the three nuclei.

II. EXPERIMENTAL DETAILS

The present measurements were performed at the Vivitron accelerator facility using a 140-MeV ^{18}O beam of intensity 2.5 pnA (with a total integrated exposure of 9.1 mC, $Q = 8^{+}$). The beam was incident on a 120 μg cm^{-2} self-supporting ^{12}C target, and inelastic scattering and transfer reactions were used to populate states in ^{18}O and ^{20,22}Ne. The breakup of the ^{18}O, ^{20}Ne, and ^{22}Ne ejectiles into ^{14}C + α, ^{16}O + α and ^{18}O + α, respectively, was detected using two charged-particle telescopes. One of the telescopes was designed to detect light ions (α particles) and the other heavy ions (carbon or oxygen nuclei). The light-ion detector was composed of three elements: a 65-μm-thick, 5 × 5 cm^2 silicon detector, a 500-μm-thick silicon-strip detector, and a 1-cm-thick CsI detector (with both the latter elements having a size equal to that of the first element). The 65-μm-thick detector was subdivided into four quadrants to minimize the detector capacitance. The strip detectors possessed 16 position-sensitive strips, each strip being 50 × 3 mm^2, with a position resolution along the strip of $\leqslant$1 mm. The energy resolution of the telescope was $\leqslant$500 keV. The heavy-ion detector telescope was composed of two elements: a gas ΔE detector and a silicon-strip stopping detector (of the same type as in the light-ion telescope). The gas was contained by a 3.5-μm-thick aluminized Mylar window and had a 5-cm-thick active volume and was operated with 75 mbar of isobutane gas. The energy and position resolutions of this telescope were similar to that of the light-ion detector

*Electronic address: M.Freer@bham.ac.uk

†Present address: Department of Chemistry, Indiana University, Bloomington, Indiana 47405, USA.

telescope, but with slightly better position resolution owing to the greater energy deposition of the heavy ions.

The resistive strip detectors in each telescope provided a measurement of the emission angle of the reaction products. For the light-ion detector the strip detector was located 143 mm from the target at an angle of 24.6° with respect to the beam axis. The strip detector element of the heavy-ion telescope was positioned 274 mm from the target at an angle of 13.0° from the beam axis on the opposite side of the beam axis to the light-ion telescope. The energy response of the telescopes was calibrated using elastic scattering of 71.4- and 102.9-MeV ^{18}O nuclei from both ^{197}Au and ^{12}C targets.

III. ANALYSIS TECHNIQUES

The three breakup reactions ^{12}C(^{18}O,^{14}C + α)^{12}C, ^{12}C(^{18}O,^{16}O + α)^{10}Be, and ^{12}C(^{18}O,^{18}O + α)^{8}Be were reconstructed using the resonant particle spectroscopy approach. The multi-element nature of the telescopes allowed ΔE-E techniques to be employed to identify oxygen and carbon nuclei in the heavy-ion telescopes (but no mass resolution was possible) and α particles in the light-ion telescopes, thus providing for some degree of channel selection. As already noted, the strip detectors provided for a determination of the emission angles of the ions and their energy—the energy loss in the gas and CsI detectors was reconstructed from the energy deposition in the strip detectors, thus improving the overall energy resolution.

These measurements were sufficient to allow a calculation of the momenta of the two detected particles, given an assumption of their masses. Then using the principle of conservation of momentum it was possible to deduce the momentum of the remaining final-state particle (the recoiling target-like particle), which went undetected. This then permitted the final-state kinetic energy to be calculated, which was linked via the beam energy to the reaction Q value,

$$E_1 + E_2 + E_{\text{recoil}} = E_{\text{beam}} + Q_3, \tag{1}$$

with $E_{1,2}$ being the kinetic energies of the two detected fragments, E_{recoil} that of the recoil, E_{beam} the beam energy, and Q_3 the three-body reaction Q value. A spectrum of the sum of the three final-state particle kinetic energies (E_{tot}) reveals the individual excitation energies of the final-state nuclei produced in the reactions.

The excitation energy (E_x) of the resonant system may be calculated from the relative velocity (v_{rel}) of the two detected decay products (with the angles of the detectors set so as to favor the kinematics of reactions in which the ejectile decayed),

$$E_x = E_{\text{rel}} + E_{\text{thresh}}, \tag{2}$$

where E_{thresh} is the associated α-decay threshold and,

$$E_{\text{rel}} = \tfrac{1}{2}\mu v_{\text{rel}}^2 \tag{3}$$

with μ being the reduced mass of the decaying system.

Finally, the angular distributions of the reaction products may provide information as to the spins of the decaying states. The experimental approach is described in detail in Ref. [14]. Briefly, the measurement of two of the three final-state particles permits the angular distributions of both the resonant particle and the two breakup products to be reconstructed. The center-of-mass (c.m.) emission angle of the resonant particle is given by the angle $\theta^\star$, and the breakup of the resonant particle is described by the angle ψ, which is the angle (in the c.m. frame of the resonant particle) between the relative velocity vector of the two fragments and the beam axis. For a reaction system in which all the initial-and final-state particles are spin zero (and for strong absorbtion in the small impact parameter region), there is a strong restriction on the reaction amplitudes and the spin of the resonant particle strongly influences the angular distributions. For the scattering angle $\theta^\star = 0^\circ$ the reaction system is constrained such that the resonant particle is populated in the $m = 0$ magnetic substate and the angular distributions $W(\theta^\star, \psi)$ are given by

$$W(0, \psi) \propto |P_J[\cos(\psi)]|^2. \tag{4}$$

For angles away from $\theta^\star = 0^\circ$ then other m substates contribute and the angular distributions are governed by associated Legendre polynomials, and the interference between these gives rise to distributions whose periodicity is determined by the Legendre polynomial of order J, but a shift in phase is introduced,

$$W(\theta^\star, \psi) \propto |P_J[\cos(\psi + \Delta\psi)]|^2, \tag{5}$$

where J is the spin of the state, and

$$\Delta\psi = \frac{l_i - J}{J}\Delta\theta^\star, \tag{6}$$

with l_i being the entrance channel grazing angular momentum (see Ref. [14]).

The analysis of the correlations is performed such that the $W(\theta^\star, \psi)$ distributions are projected onto the $\theta^\star = 0^\circ$ axis at an angle defined by $\Delta\theta^\star/\Delta\psi$. The periodicity of the resulting projection is then compared with Legendre polynomials of order J, the spin of the decaying state. The projection angle, which is also sensitive to the spin, and the periodicity must be consistent for a spin assignment to be made.

IV. RESULTS

A. Breakup of ^{18}O

Figure 1 shows the total final-state kinetic energy spectrum for ^{14}C + α coincidences. The Q value for the ^{12}C(^{18}O,^{14}C + α) reaction is −6.227 MeV, and thus the peak corresponding to all of the reaction products in their ground states should lie at a total energy of 133.8 MeV (indicated by the vertical line in the upper part of Fig 1). The highest energy peak is found at an energy of 134.1 MeV (i.e., within 300 keV of that expected), with a width that is determined by the experimental resolution (FWHM) of 1.7 MeV. The peaks at lower total energies lie 4.4, 7.1, and 11.9 MeV below the highest energy peak. The first two of these would correspond to the excitation of the ^{12}C recoil particle (4.4 MeV, 2^+) and ^{14}C breakup particle (7.01 MeV, 2^+). The third peak results from mutual ^{12}C + ^{14}C excitations. The excitation energy spectrum corresponding to the events highlighted in Fig. 1(a) is shown in Fig. 1(b). The spectrum extends from the experimental threshold (as indicated by the

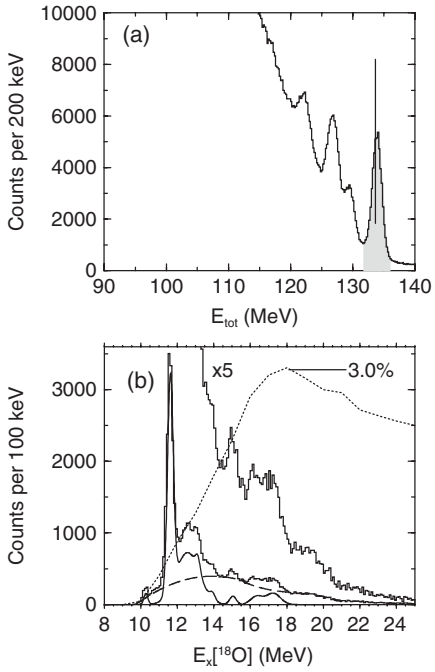

FIG. 1. (a) The calculated total energy spectrum for the ^{12}C(^{18}O,^{14}C + α)^{12}C reaction. The shaded region shows the events selected for the ^{14}C + α decay of ^{18}O. The vertical line indicates the *theoretical* position of the peak corresponding to the three final-state particles being produced in the ground state (133.8 MeV). (b) The excitation energy spectrum for ^{18}O → ^{14}C + α decays. The high excitation energy region is shown multiplied by a factor of 5 to emphasize the structure in this portion of the spectrum. The dotted line shows the experimental detection efficiency calculated using Monte Carlo simulations of the reaction and detection processes (with the maximum value indicated). The smooth line to corresponds to the peak-fit analysis (the peak component), and the long-dashed line to the extracted background.

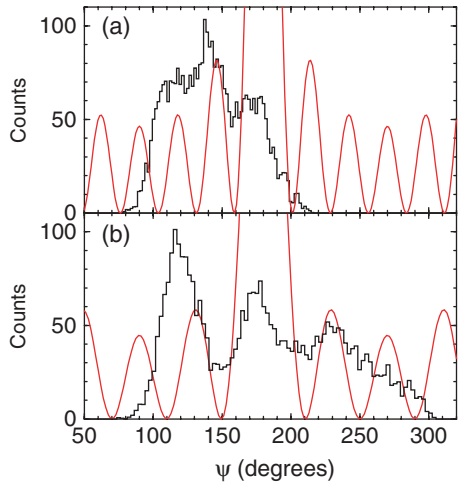

FIG. 2. (Color online) Angular distribution for the breakup of ^{18}O to ^{14}C + α for the ^{18}O excited state at (a) 12.61 MeV and (b) 13.11 MeV. The smooth line in (a) corresponds to the function $|P_6(\cos\psi)|^2$ and in (b) to $|P_4(\cos\psi)|^2$. An agreement between the periodicity of the data and the Legendre polynomial would suggest $J^\pi = 6, 4^+$, respectively. Note, however, that in the case of the 12.61-MeV data the correlations are equally well described by spins of 2, 4, and 6. For the 13.11-MeV peak the decay of a spin 4 state provides the best description of the data, although spin 2 cannot be excluded.

Monte Carlo simulations of the detection efficiency) at 10 MeV (the decay threshold being 6.227 MeV) up to 23 MeV. The excitation energy resolution has been predicted by simulations of the reaction and detection processes (including the energy and position resolution of the detectors and energy loss and energy and angular straggling in the target). These calculations predict that the resolution (FWHM) should be 350 keV at E_x = 10 MeV, increasing to 500 keV at E_x = 15 MeV. The widths of the observed peaks are close to these values, indicating that the true widths of the states are not being probed. The spectrum of states observed is essentially the same as observed in the ^{14}C(^{18}O,^{14}C + α) [12] and ^{9}Be(^{18}O,^{14}C + α) [13] reactions and are listed in Table I.

The peaks at 10.29, 11.63, 12.61, and 13.11 MeV agree with the previous measurements of Curtis [12] and Ashwood [13] within 50 keV for the first two states and within 140 keV for the higher energy states. The agreement with the tabulations of Tilley *et al.* [15] is also of a similar quality. The overlap in the possible spins of the 10.29-MeV state observed in the ^{14}C(^{18}O,^{14}C + α) reaction [12] and the tabulated value of 4^+, and the definite assignment of 5^- to the 11.62 MeV breakup state, which agrees with the tabulated spin of the 11.62-MeV state, provides confidence in both the calibration of the excitation energy and in the correct identification with the states in the tabulations of ^{18}O. The spin analysis of the present data cannot provide a very stringent limit on the spins of the 10.29-and 11.63-MeV states. In the case of the two peaks at 12.61 and 13.11 MeV the analysis of the angular correlations limited the spins, and thus parities, to being even. The established J^π of the 12.53-MeV state concurs with the possible 6^+ assignment deduced in the present analysis. In the case of the peak at 13.11 MeV, which we associate with the 13.00-MeV state in the data of Curtis *et al.*, the analysis of the angular distributions cannot unambiguously distinguish between $J + 2$ or 4, though a spin of 4 is favored. Figure 2 shows the angular correlation for the peak at 13.11 MeV projected at an angle that would coincide with an entrance channel grazing angular momentum of $l_i = 32\hbar$ [see Eq. (5)]. We note that in the analysis of the angular correlations for the 11.62-MeV 5^- state in the ^{14}C(^{18}O,^{14}C + α) reaction at 102 MeV [12] the l_i was found to be $31\hbar$. A calculation of the grazing angular momentum for the present reaction and beam energy, scaled to that determined for the 11.62-MeV state, suggests a value of $32\hbar$, in agreement with the present analysis.

In the higher excitation energy portion of the spectrum in Fig. 1(b) we find evidence for peaks at 15.04 and 17.40 MeV, which do not appear to correspond with any observed in the two earlier studies [12,13]. The 16.20-MeV peak may correspond to the 16.42-MeV peak in [12]. The 17.40-MeV peak may be linked to the 17.05-MeV 7^- state, which was observed in the ^{14}C(^{6}Li,*d*) reaction [16]. The correlations for these higher lying states did not produce conclusive spin assignments.

TABLE I. States observed in the present $^{12}C(^{18}O,^{14}C+\alpha)$ reaction study and other inelastic break-up studies [12,13]. These are compared to the states listed in the tabulations of Tilley *et al*. [15]. Note that only states with natural parity and spin assignment are shown from Ref. [15].

Tilley *et al*. [15]			$^{14}C(^{18}O,^{14}C+\alpha)$ [12]		$^{9}Be(^{18}O,^{14}C+\alpha)$ [13]		Present work	
E_x (MeV)	J^π	Γ (keV)	E_x (MeV)	J^π	E_x (MeV)	Γ (keV)	E_x (MeV)	J^π
6.404	3^-	30 ± 15 fsec						
7.117	4^+	<25 fsec						
7.619	1^-	<2.5						
7.864	5^-		7.86					
8.038	1^-	<2.5	8.04					
8.125	5^-							
8.213	2^+	1.0 ± 0.8	8.22					
8.282	3^-	8 ± 1						
8.955	(4^+)	43 ± 3						
9.0	(1^-)							
9.361	2^+	27 ± 15	9.35	$(2^+, 3^-)$	9.39(5)			
9.672	(3^-)	60 ± 30	9.70	$(1^-, 2^+, 3^-)$	9.72(5)			
10.118	3^-	16 ± 4						
10.295	4^+		10.29	$(3^-, 4^+, 5^-)$	10.27(5)		10.29	
10.396	3^-							
11.39	(2^+)							
11.41	(4^+)							
11.62	5^-	76 ± 8	11.62	5^-	11.58(5)		11.63	
11.67	(3^-)							
11.69	6^+							
11.82	(3^-)							
12.04	(2^+)	28 ± 6	12.06					
12.25	(1^-)							
12.33	5^-							
12.41	(3^-)							
12.50	4^+							
12.53	6^+		12.54		12.47(5)	<300	12.61	$(2^+,4^+,6^+)$
			13.00	$(2^+, 4^+)$	13.04(5)		13.11	$(2^+,4^+)$
13.1	1^-	700						
13.8	1^-	600						
					13.8(1)	<480	13.94	
14.7	1^-	800	14.58					
							15.04	
					15.7(1)	<360		
15.8	1^-	700	15.46					
16.315	$(2,3)^-$	~600	16.42				16.20	
					16.8(1)	<300		
16.948	$(2,3)^-$	<20						
17.05	(7^-)[a]	~350					17.40	

[a]The states at 17.05 and 18.95 MeV populated in the $^{14}C(^6Li, d)$ reaction have been assigned $J^\pi = 7^-$ by Artemov *et al*. [16].

B. Breakup of ^{20}Ne

The total energy spectrum for the $^{12}C(^{18}O,^{16}O+\alpha)$, $2p$-transfer reaction is shown in Fig. 3(a). The Q value for this reaction is -11.08 MeV, and thus the peak corresponding to the production of all three final-state particles in the ground state should lie at 128.9 MeV, as indicated by the solid vertical line. The observed peak is found to lie within 200 keV of that calculated. Two peaks are also found at lower total energies—3.34 and 6.49 MeV below the highest energy peak. The first of these predominantly arises from excitation of the ^{10}Be recoil (3.34 MeV, 2^+); the peaks in the excitation energy spectra for the ground state and 3.34-MeV total energy peaks are similar. The character of the second peak cannot be uniquely identified as it corresponds to the excitation of only a group of states in ^{16}O and ^{10}Be in the 6- to 7-MeV excitation energy region.

The excitation energy spectrum corresponding to the three final-state particles being in the ground state is shown in Fig. 3(b) [corresponding to the shaded region in Fig. 3(a)].

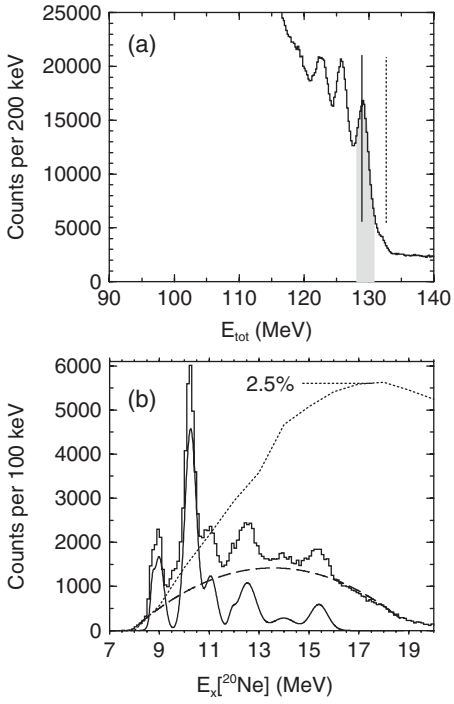

FIG. 3. (a) Total energy spectrum for the ^{12}C(^{18}O,^{16}O + α)^{10}Be reaction. The shaded region shows the events selected for the calculation of the excitation energy of the ^{16}O + α decay of ^{20}Ne. The solid vertical line indicates the *theoretical* position of the peak corresponding to the three final-state particles being produced in the ground state (128.9 MeV). The dotted line indicates the position of the ^{12}C(^{18}O,^{18}O + α) reaction (132.6 MeV). (b) The excitation energy spectrum for ^{20}Ne → ^{16}O + α decays. The dotted line shows the calculated experimental detection efficiency; the maximum value is indicated. The smooth solid line to corresponds to the peak-fit analysis (the peak component), and the long-dashed line to the extracted background.

The strongest states observed are listed in Table II. The lower excitation energy limit is defined by the experimental acceptances (as indicated by the Monte Carlo simulations). As in the case of the ^{18}O data, there is very good agreement between the peak centroids extracted here and the tabulations of Tilley *et al*. [17]. The agreement is within 50 keV for the lower energy states and increasing to 80 keV at 15.44 MeV.

An analysis of the angular correlations of the peaks observed in the ^{20}Ne excitation energy spectrum was used to establish the correspondence between the states observed in the present study and those in the tabulations. In the case of the 8.77- and 9.04-MeV peaks the correlation data were limited by the experimental acceptance, and definite spin determinations were not possible. Nevertheless, if the correlation distributions were projected at an angle consistent with the value of $l_i = 32\hbar$ found in the analysis of the breakup of ^{18}O, the two correlations were found to be consistent with $J^\pi = 4^+$ and 6^+, respectively. The correlations for the peaks at 10.28, 12.53, and 15.44 MeV were not so limited and assignments of $J^\pi = 5^-$, 6^+, and 7^-, respectively, were made (see Fig. 4). The correlations for the peaks at 11.03, 11.96, and 14.04 MeV were largely featureless, which is characteristic of either low spin states or, alternatively, the contribution from two states with differing spins, and thus definite assignments to states in the tabulations of Tilley *et al*. [17] were not possible; in these cases the most likely candidates have been listed.

TABLE II. States observed in ^{20}Ne for the reaction ^{12}C(^{18}O, ^{16}O + α). The energies and spins measured in the present work are compared with those listed in Ref. [17], and with the $T = 0$ states from the reaction ^{18}O(^{3}He,*n*)^{20}Ne [18,19].

Present work		Tilley *et al*. [17]		^{18}O(^{3}He,*n*)^{20}Ne [18,19]	
E_x (MeV)	J^π	E_x (MeV)	J^π [band]	E_x (MeV)	J^π
				7.86	
8.77	(6$^+$)	8.7776	6$^+$ [0$^+_1$]		
				7.79	
9.04	(4$^+$)	9.031	4$^+$ [0$^+_3$]		
				9.05	
				9.98	
10.28	5$^-$	10.262	5$^-$ [0$^-$]		
				10.88	
11.03		(10.97, 11.020)	(0$^+$, 4$^+$)		
				11.27	
				11.48	(0$^+$)
				11.59	
11.96		(11.951)	(8$^+$; [0$^+_1$])		
				12.21	2$^+$
				12.41	0$^+$
12.53	6$^+$	12.585	6$^+$ [0$^+_2$]		
				12.83	
				13.10	0$^+$
				13.34	
				13.48	
				13.59	(2$^+$)
				13.90	(2$^+$)
14.04		(14.02, 14.063)	(1$^-$, 2$^+$)		
				14.22	
15.44	7$^-$	15.366	7$^-$		

The states observed in the only other two-proton (2*p*) transfer reaction listed in Ref. [17] are also shown in Table II [18,19]. We note that the agreement between the two sets of data is not particularly good. In fact it is difficult to identify states seen in both reactions. This may reflect the fact that the contribution of isospin to the two reactions is different (by virtue of the decay channel selected, the present measurements sample only $T = 0$ states in ^{20}Ne) and that the angular momentum transfer is much larger in the present measurements owing to the larger c.m. energy (the earlier measurements being limited to low spin states). Thus, the present studies are complementary to the earlier measurements, as they provide information on the population of higher spin states in the two-proton transfer reaction.

C. Breakup of ^{22}Ne

As has been shown in the preceding analysis, the vast majority of the oxygen-α coincidences in the total energy region $E_{tot} > 120$ MeV can be accounted for by the decay

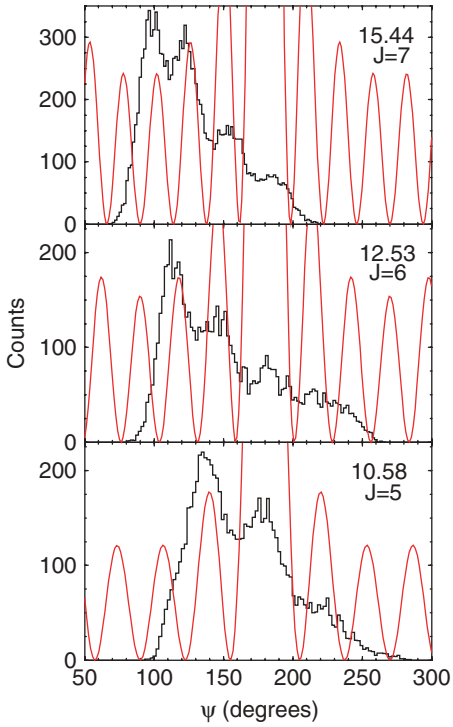

FIG. 4. (Color online) Angular distributions for the breakup of ^{20}Ne to ^{16}O + α for the states at 10.28, 12.53, and 15.44 MeV. The lines show the periodicity of Legendre polynomials of order 5, 6, and 7, suggesting $J^{\pi} = 5^{-}$, $6,^{+}$ and 7^{-}.

of ^{20}Ne to ^{16}O + α. The Q value for the ^{12}C(^{18}O,^{18}O + α)^{8}Be reaction is −7.37 MeV, 3.7 MeV more positive than that for the ^{12}C(^{18}O,^{16}O + α)^{10}Be reaction. The corresponding total energy is indicated by the vertical dotted line in Fig. 3(a), where a small shoulder appears on the highest energy peak associated with the ^{20}Ne breakup. It should be noted that there is no such feature present in the spectrum in Fig. 1(a). It is interesting that although the 2p-transfer and α-transfer reactions would be expected to have similar cross sections, the α transfer is significantly suppressed with respect to the 2p transfer. The α-transfer cross section is less than 10% of that for the 2p transfer (even though the Q value is more positive). Assuming a detection efficiency of 1% (which is approximately the efficiency calculated for the regions in which the peak in strength in the excitation energy spectra are located), the cross sections for the three reactions populating ^{18}O, ^{20}Ne, and ^{22}Ne are 96(1), 161(1), and 12(1) μb, respectively.

The ^{22}Ne excitation energy spectrum has been calculated by selecting events that lie in the region of the shoulder in Fig. 3(a) and is shown in Fig. 5. The spectrum suggests the presence of a number of states between 15 and 22 MeV. An analysis of the peak identified with the breakup of ^{20}Ne, but assuming the ^{18}O + α decay channel, broadens the peaks in the ^{20}Ne excitation energy spectrum. The large peak at 10.28 MeV in Fig. 3(b) then coincides with the broad feature seen in Fig. 5 close to 15 MeV. Thus, there may be a small contamination of the spectrum in this region from the ^{16}O + α decay. The remainder of the peaks in the ^{20}Ne excitation energy spectrum do not coincide with those

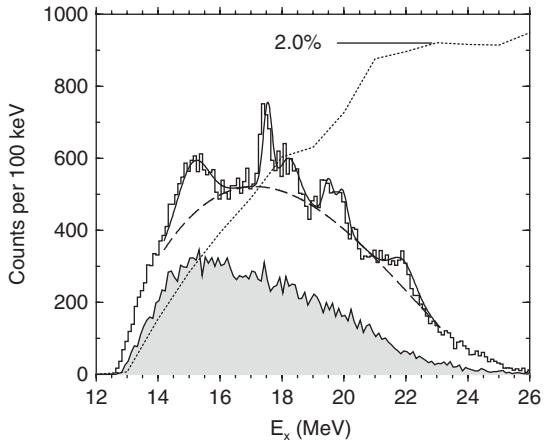

FIG. 5. The ^{22}Ne excitation energy spectrum gated on the region indicated by the vertical dotted line in Fig. 3. The shaded spectrum corresponds to a gate of the same width in energy (1.7 MeV) placed on the background region of the total energy spectrum close to 137.5 MeV. The dotted line shows the calculated detection efficiency. The smooth line corresponds to the peak-fit analysis, and the long-dashed line to the extracted background.

observed in Fig. 5. However, there is a large component in this spectrum that arises from the background and is observed to extend to high total energies in Fig. 3, this component arises from α-particle pileup in the heavy-ion telescope. The shaded spectrum in Fig. 5 shows the reconstructed excitation energy spectrum for a gate of the same width as that used to create the ^{22}Ne spectrum, but for events at higher E_{tot}. It can be seen that the background spectrum contains none of the structure present in the ^{22}Ne excitation energy spectrum, indicating that the features observed are genuine peaks. The states observed in the present measurements are compared with those observed in the earlier breakup measurement [12] and resonant ^{18}O + α elastic scattering measurements [9] in Table III.

Figure 6 displays the analysis of the spins for the three peaks that were associated with structured angular correlations. The remaining peaks are probably associated with multiple states with different spins, leading to the suppression of the angular correlation ridge pattern. The quality of the correlation patterns do not match those found for the analysis of the breakup of ^{20}Ne owing to both the limited statistics and the significant background contribution. They do, however, give some indication of the spin, and owing to the overlap of the correlation pattern with the $\theta^{\star} = 0^{\circ}$ axis at $\psi = 90^{\circ}$, for which the correlation amplitude is zero for negative parity and a maximum for positive parity [a property of the Legendre polynomials $P_J(\cos\psi)$], the parity may be assigned for the three states. This latter analysis is independent of the projection angle, the uncertainty in which leads to the ambiguity in the spin assignment. For the three states at 19.45, 19.89, and 21.96 MeV the correlations have been projected at an angle defined by the entrance channel grazing angular momentum $l_i = 32\hbar$ and the spins shown in Fig. 6. The data suggest that the spins of the three states are 6^{+}, 10^{+} and 9^{-}, respectively.

In the case of the 21.96-MeV peak, this is most probably the 21.84-MeV 9^{-} resonance observed in the ^{18}O + α resonant

TABLE III. Summary of states observed in ^{22}Ne. The present measurements are compared with those for the ^{14}C(^{18}O,^{18}O + α) reaction [12] and ^{18}O + α resonant scattering measurements [9]. The brackets for the present spin determinations indicate tentative spin assignments; the parities have, however, been determined in each case (see text). Owing to the large background (Fig. 5) the uncertainties on the peak centroids is ±100 keV.

Present work		^{14}C(^{18}O,^{18}O + α) [12]	^{18}O + α [9]			
E_x (MeV)[a]	J^π	E_x (MeV)	E_x (MeV)	J^π	$\gamma_\alpha^2/\gamma_W^2$ (%)	$\Gamma_\alpha/\Gamma_{\rm tot}$ (%)
			12.58	1^-	10	36
			12.84	1^-	20	72
		(12.8)				
			13.19	3^-	19	40
			13.41	3^-	11	40
		14.27, 14.47				
(15.05)[b]						
		15.2				
		16.45				
17.48						
		(17.8)				
18.42						
		(18.7)				
			19.28	7^-	8	25
19.45	$(6)^+$					
			19.56	7^-	5	23
19.89	$(10)^+$	(19.9)				
		(20.8)	20.85	9^-	51	14.5
21.96	$(9)^-$	(22.2)	21.84	9^-	57	22

[a]The uncertainty in the excitation energy is ±100 keV.
[b]This is only a tentative assignment as it coincides with a possible contaminant from the decay of ^{20}Ne to ^{16}O + α.

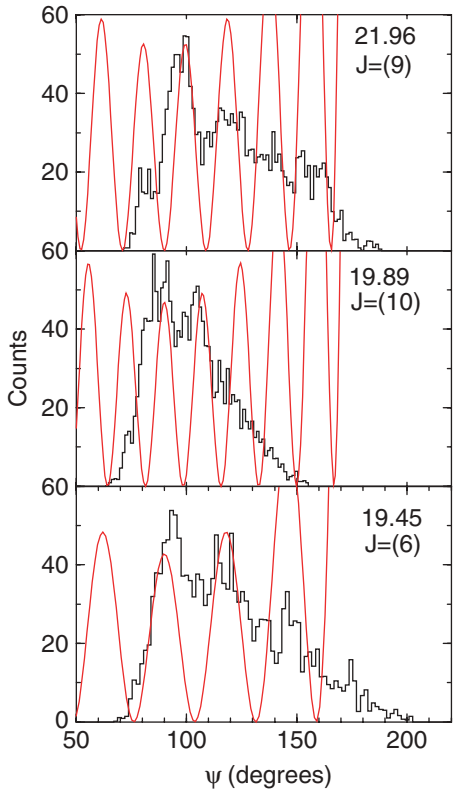

FIG. 6. (Color online) The ^{22}Ne correlation analysis for states that possess structured angular correlations. Owing to the limited statistics and significant background contributions only tentative spin assignments were possible. Because the correlations intercept the $\theta^\star = 0^\circ$ axis close to $\psi = 90^\circ$, the parity could be definitely assigned (see text).

scattering measurement of Ref. [9]. It is interesting that over the energy range sampled in the present measurements only negative-parity states were observed in the resonant scattering measurements. In the measurement of the ^{14}C(^{18}O,^{18}O + α)^{10}Be reaction the experimental threshold was lower than in the present case, and the state at 14.47 MeV was dominant. This state is suppressed here owing to the reduced detection efficiency at this energy. The broad bump observed close to 15 MeV in Fig. 5 may correspond to a series of unresolved states, as indicated by the correlation analysis, which may, in part, include the state at 14.47 MeV.

V. DISCUSSION

A. ^{18}O

In Ref. [13] it was suggested that the negative-parity states populated in the inelastic scattering breakup reaction could be linked to the $(sd)^1(fp)^1$ configuration. The 5^- state is the strongest state populated in this reaction and no candidate for the 7^- state was found. It was proposed in Ref. [13] that the 5^- state was thus the termination of the negative-parity $K^\pi = 0^-$ band, which, for a single neutron in both the *sd* and *fp* shell, cannot exceed a spin of 5. In the present measurement the c.m. energy is 25% higher than in the work of Curtis *et al*. [12] and 13% higher than in that of Ashwood *et al*. [13]. An increase in the c.m. energy would allow the population of higher spin states. There is, however, still no indication of a 7^- state at higher energy, supporting the band termination hypothesis.

Measurements of the resonant scattering of ^{4}He on ^{14}C have provided information on the spins and α-decay widths (Γ_α) and total widths (Γ) of resonances up to an excitation energy of 22 MeV [20]. These systematics are plotted in Fig. 7, where the size of the symbol indicates the magnitude of Γ_α/Γ for each resonance. (Note that only resonances with definite spins are plotted.) These measurements indicate that there are a number of resonances with a strong α-cluster structure (values of Γ_α/Γ that are close to 1). The states of the negative-parity band (9.672 MeV, 3^- and 11.62 MeV, 5^-) found in the present inelastic scattering breakup reaction and in [12,13] are among them—the 8.038-MeV 1^- resonance was not studied in Ref. [20]. The resonant scattering measurements did not provide any evidence for a 7^- member, which as shown by the dotted line would lie close to 15 MeV. However, this is the region of ^{18}O excitation energy where there was no sensitivity (as indicated by the horizontal dashed lines). Measurements

of the transfer reaction ^{14}C(^{6}Li,d)^{18}O [16,21], however, found two 7^- states, but these lie at 17.05 and 18.95 MeV and are therefore probably too high in energy to form the extension of the aforementioned negative-parity band. Thus, the band termination hypothesis appears to be confirmed by the transfer studies.

There, thus, remains the question as to the origin of the 17.05-and 18.95-MeV 7^- states, both of which are strongly populated in the α transfer. The 12.33-MeV 5^- state is also populated in the α-transfer reaction [21] (reported at a slightly higher energy of 12.6 MeV in the measurements of Artemov *et al*. [16]). These states may be linked to the 3^- and 1^- states at 8.282 and 6.198 MeV, respectively, both of which are also populated in the α-transfer measurements [21].

In Ref. [13] it was suggested that the negative-parity band connected with the 8.038-MeV 1^- state was the analog of the $K^\pi = 0^-$ band in ^{20}Ne and that this was the partner band to the $K^\pi = 0^+$ ^{18}O ground-state band forming the analog of the octupole configuration ^{20}Ne [5]. A 0^- (0_2^-) cluster band was found in the multiconfigurational Generator Co-ordinate Method (GCM) calculations of Descouvemont and Baye [22], which also terminates at a spin of $J = 5$, which is almost certainly associated with the present band. In ^{20}Ne both the $K^\pi = 0^\pm$ bands have a well-developed cluster structure. For the positive-parity states observed in the α-transfer reaction, the most strongly populated state is the 4^+ 7.11-MeV level. This state is a member of the 4p-2h band, which is linked to the sequence of states 0^+ (3.63 MeV), 2^+ (5.24 MeV), 4^+ (7.11 MeV), and 6^+ (11.69 MeV) [23]. This band corresponds to the transfer of the α particle to the *sd* shell and should extend to a maximum spin of 8^+, and the 8^+ state observed in the resonance scattering studies at 20.227 MeV [20] may be the terminating state in this band (the lower solid line in Fig. 7).

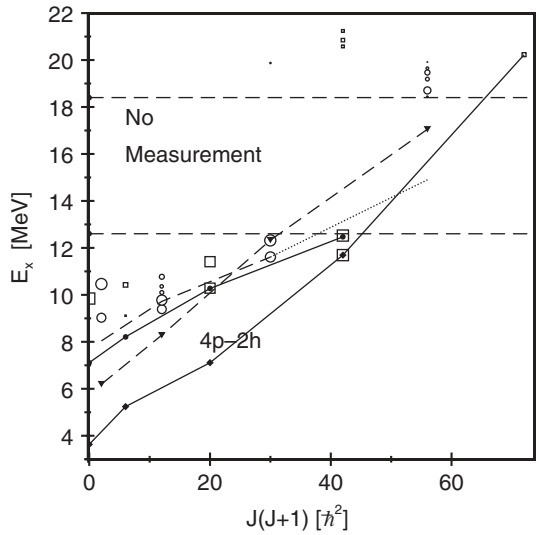

FIG. 7. The energy-spin systematics of resonances in ^{18}O. The open symbols show the states observed in the ^{4}He + ^{18}O resonance scattering study [20]. Positive- and negative-parity resonances are indicated by the open squares and open circles, respectively. The size of the symbol is proportional to the value of Γ_α/Γ. The horizontal dashed lines indicate the region in which there were no measurements. Bands of positive and negative parity, referred to in the text, are indicated by solid and dashed lines, respectively.

There is one other positive-parity band that was identified by Fortune [23] with the $6p$-$4h$ configuration. The suggested $6p$-$4h$ band corresponds to the states 0^+ [7.11 MeV], 2^+ (8.21 MeV), 4^+ (10.29 MeV), and 6^+ (12.53 MeV), which are observed in the present measurements. It should be noted that the 7.11-MeV 0^+ state has not been observed but was postulated by Fortune [23] and coincides with the known 4^+ state at the same energy. The higher energy members of this band are observed in the resonant scattering studies to have a large cluster content [20]. However, $6p$-$4h$ states would not be expected to be strongly populated in the resonant scattering or in the ^{14}C(^{6}Li,d) transfer studies. In the present measurements $6p$-$4h$ ^{18}O states would not strongly decay to the $^{14}C_{gs} + \alpha$ final state. They should, instead, decay to ^{14}C excited states. We conclude therefore that the $6p$-$4h$ assignment is not well founded. The positive-parity band observed in the inelastic scattering breakup reactions can be associated with the $K = 0_4^+$ band (0^+ 8.7 MeV, 2^+ 9.0 MeV, 4^+ 10.8 MeV) with a $4p$-$0h$ excitation to the *fp* shell [3]. This band lies at a similar excitation energy. Therefore it is probable that the present ^{18}O band corresponds to the $4p$-$2h$ excitation with an α particle in the *fp* shell, and not the $6p$-$4h$ configuration.

The positive-parity states are observed up to $J^\pi = 6^+$, but recoupling the angular momenta of the valence particles in the *fp* shell could produce spins up to 12^+. It is possible that some of the more weakly populated states at higher excitation energy ($E_x \geqslant 13$ MeV) are associated with the continuation of the band but owing to their higher spin are much more weakly populated. In addition, the spin analysis of the present measurements and those of Curtis *et al*. suggest that the 13.11-MeV state (13.00 MeV in Ref. [12]) has spin and parity (2^+, 4^+). This state would thus not fall onto the systematics of the bands already mentioned, and thus it is equally possible that the higher excitation energy states are linked to an alternate structure in common with that associated with the 13.11-MeV state. Indeed, Fig. 7 indicates that there are several levels with significant α widths that have not been placed in the present systematics.

B. ^{20}Ne

The states in ^{20}Ne have been classified into bands, the corresponding structures of which have been established [3]. The bands have been identified with the following shell-model configurations:

(i) 0_1^+: $(sd)^4$,
(ii) 2^-: $(p)^{-1}(sd)^5$,
(iii) 0_2^+: $(sd)^4$,
(iv) 0_3^+: $(p)^{-4}(sd)^8$,
(v) 0_4^+: $(fp)^4$, and
(vi) 0^-: $(sd)^3(fp)^1$.

We expect that in the $2p$ transfer the states associated with the $K^\pi = 0_1^+$, 0_2^+, 0_3^+, and 0^- configurations will be dominant. Indeed (as indicated in Table II) the states of

such configurations are excited. It should be noted that the strengths of the states observed in the present excitation energy spectrum is, beyond acceptance effects, a function of both the excitation and decay probabilities. Thus, the population of the bands is modulated also by their α-cluster content. In this respect the $K^\pi = 0_1^+, 0^-$, and 0_4^+ bands are believed to possess well-developed cluster structures [3].

In the case of the 0_1^+ band we observe the 6^+ state at 8.77 MeV and possibly the 8^+ state at 11.95 MeV. The 0_2^+ band's 6^+ state at 12.585 MeV is clearly seen and the associated 4^+ state may correspond to the low-energy shoulder on the 10.28-MeV peak. Finally, the 5^- member of the $K^\pi = 0^-$ band is the strongest feature of the spectrum, but there is little evidence for the 13.69-MeV 7^- member.

The strong population of the 5^- member of the $K^\pi = 0^-$ band would in part be explained by the well developed α-cluster structure of this state, enhancing the decay probability. The nonobservation of the 7^- member could be explained by the maximum spin that can be generated from the transfer of one nucleon to both the *sd* and *fp* shells ($6\hbar$). This suggests that recouplings in the ^{18}O core do not play a dominant role in the reaction. In the case of the ground-state band, where the 6^+ and 8^+ members are seen, recoupling of the valence neutrons in ^{18}O is required to generate the observed spin, and this would explain their weaker population.

The 2^- and 0_4^+ bands are not observed, as expected, because in the former case the ^{16}O closed shell must be excited, and in the latter the two valence neutrons in ^{18}O must be excited to the *fp* shell—these are both second-order processes.

Interestingly, members of the 0_3^+ band are observed $[(p)^{-4}(sd)^8]$. The 4^+ member of the 0_3^+ state is seen at 9.031 MeV and there may be a contribution to the 12.53-MeV peak (which is much broader than would be expected based on the experimental resolution) from the 12.137-MeV 6^+ state. This would indicate that either $4p$-$4h$ excitations of the ^{16}O core of ^{18}O play an important role (but again this would be expected to be a second-order process). Alternatively, it may be that the structure of the 0_3^+ band is much more complex than a simple $(p)^{-4}(sd)^8$ configuration and contains important components from other *sd*-shell configurations.

C. ^{22}Ne

Using the $^{18}\mathrm{O} + \alpha$ resonant scattering reaction [9], a number of resonances in ^{22}Ne were observed in the excitation energy range probed here. Their properties are listed in Table III. Most significantly, it was observed that a negative-parity band was the strongest feature, with the 1^-, 3^-, 7^-, and 9^- members (the 5^- states being unobserved) forming a set of doublets. This band was believed to be the analog of the $K^\pi = 0^-$ band in ^{20}Ne [9]. In ^{18}O the negative-parity $K^\pi = 0^-$ band would have the configuration $(sd)^1(fp)^1$ and in ^{20}Ne $(sd)^3(fp)^1$. Thus, given that the negative-parity band in ^{22}Ne mirrors that in ^{20}Ne [9] the band may have a $(sd)^5(fp)^1$ configuration. In the current measurements we observe the 9^- state with the largest α-decay width (21.84 MeV), and possibly some of the yield close to 20.85 MeV may be associated with the other member. The two 7^- states in the resonant scattering measurements are located close to an energy where we claim the parity is positive and the correlations may reflect $J = 6$. Nevertheless, the quality of the data is such that we cannot exclude some $J = 7$ contribution. The 3^- states are at the low-E_x extreme of the present excitation energy spectrum and thus are suppressed by the reduced detection efficiency. The present measurements provide no evidence for 5^- states. In addition to the negative-parity states, we observe states of positive parity not identified in Ref. [9].

The most striking feature of the data is the very small cross section for the population of states in ^{22}Ne, a feature also observed in two previous measurements of α transfer onto ^{18}O from ^{14}C [12] and ^{9}Be [13] targets. In part this will be linked to the α-decay widths of the states. As can be seen from Table III, for the negative-parity states the reduced widths compared to the Wigner limit are found to be significant [9] for the 9^- states, but the α-decay width is reduced by the presence of the centrifugal barrier. For the lower spin states the $\gamma_\alpha^2/\gamma_W^2$ ratios are smaller, indicating a less well developed cluster structure. Thus, it is possible that the small cross section observed here is linked to the fact that the states do not have a dominant $\alpha + {}^{18}\mathrm{O}_{\mathrm{gs}}$ cluster structure. It is also possible that the excitation process has a strong influence on the cross section. However, simple angular momentum matching estimates suggest that, over the region of excitation energy probed (10–22 MeV), the population of states with spins $(5$–$8)\hbar$ would be favored, close to those expected from the resonant scattering studies. Thus, we would conclude that the most significant differences between the ^{20}Ne and ^{22}Ne decays in the present work are a reflection of the α-cluster decay widths of the states, whereby the cluster structure is suppressed in ^{22}Ne compared with that in ^{20}Ne.

This conclusion agrees well with the systematics from lithium-induced reactions. Experimental data on the d, t, and α-cluster transfer in the (^{6}Li,α), (^{7}Li,α), (^{6}Li,d), and (^{7}Li,t) reactions on light nuclei show that very strong transitions are only observed if the target has an entirely empty *sd* shell [24]. And vice versa: The cross sections for α transfer fall off sharply with increasing number of nucleons in the *sd* shell. This suggests that the residual interaction of the valence nucleons to a large extent destroys the cluster structure at the nuclear surface.

VI. SUMMARY AND CONCLUSIONS

The reactions $^{12}\mathrm{C}(^{18}\mathrm{O},^{14}\mathrm{C}+\alpha)^{12}\mathrm{C}$, $^{12}\mathrm{C}(^{18}\mathrm{O},^{16}\mathrm{O}+\alpha)^{10}\mathrm{Be}$, and $^{12}\mathrm{C}(^{18}\mathrm{O},^{18}\mathrm{O}+\alpha)^{8}\mathrm{Be}$ have been used to investigate α-decaying states in the nuclei ^{18}O, ^{20}Ne, and ^{22}Ne populated through inelastic scattering and $2p$ and α transfer, respectively. Analysis of the angular correlations of the decay products was used to confirm the energy-spin systematics of earlier studies. In the case of ^{18}O, an analysis of the results from inelastic scattering, resonance scattering, and α transfer has been used to arrange the states into rotational bands that have well-developed cluster structures. These bands are found to be the analogs of those in ^{20}Ne. This mirroring of cluster states in ^{18}O and ^{20}Ne may be traced to the common features of ^{14}C and ^{16}O, which form the basis for the corresponding

core + α cluster systems. Both ^{14}C and ^{16}O have very similar level structures, indicating the strong influence of the neutron closed shell in ^{14}C. Thus, it appears that ^{14}C behaves as a closed-shell ^{16}O nucleus in states in ^{18}O with large cluster parentages. An analysis of the cluster bands populated by the $2p$ stripping onto ^{18}O provided good agreement with the adopted configurations for the $K^\pi = 0^+_1, 2^-, 0^+_2, 0^+_4,$ and 0^- bands in ^{20}Ne. However, the data suggested that the proposed $(p)^{-4}(sd)^8$ configuration for the 0^+_3 band may be mixed with other $(sd)^4$ configurations. Finally, the analysis of the states in ^{22}Ne populated in the α transfer onto the ^{18}O indicated that the reaction proceeded with an anomalously small cross section and this was interpreted as arising from a reduced degree of $^{18}O_{gs} + \alpha$ clusterization in ^{22}Ne.

ACKNOWLEDGMENTS

We would like to acknowledge the efforts of the Vivitron operations staff and the support provided by Florent Haas. MF acknowledges financial support from the Alexander von Humboldt Foundation, which supported part of this work.

[1] R. R. Betts, in *Proceedings of Sixth International Conference on Cluster in Nuclear Structure and Dynamics, Strasbourg, Sept. 6–9 (1994)*.
[2] D. A. Bromley, in *Proceedings of the Fourth International Conference on Clustering Aspects of Nuclear Structure and Nuclear Reactions, Chester, United Kingdom*, edited by J. S. Lilley and M. A. Nagarajan (Reidel, Dordrecht, 1985), p. 1.
[3] T. Tomoda and A. Arima, Nucl. Phys. **A303**, 217 (1978).
[4] S. J. Sanders, L. M. Martz, and P. D. Parker, Phys. Rev. C **20**, 1743 (1979).
[5] H. Horiuchi and K. Ikeda, Prog. Theor. Phys. A **40**, 277 (1968).
[6] P. A. Butler and W. Nazarewicz, Rev. Mod. Phys. **68**, 350 (1996).
[7] Y. Kanada En'yo and H. Horiuchi, Prog. Theor. Phys. **93**, 115 (1995).
[8] S. Thummerer *et al*., J. Phys. G **29**, 509 (2003).
[9] G. V. Rogachev *et al*., Phys. Rev. C **64**, 051302(R) (2001).
[10] V. Z. Goldberg *et al*., Phys. Rev. C **69**, 024602 (2004).
[11] Y. Alhassid, M. Gai, and G. F. Bertsch, Phys. Rev. Lett. **49**, 1482 (1982); M. Gai, R. Keddy, D. A. Bromley, J. W. Olness, and E. K. Warburton, Phys. Rev. C **36**, 1256 (1987); M. Gai, M. Ruscev, D. A. Bromley, and J. W. Olness, *ibid*. **43**, 2127 (1991).
[12] N. Curtis, D. D. Caussyn, C. Chandler, M. W. Cooper, N. R. Fletcher, R. W. Laird, and J. Pavan, Phys. Rev. C **66**, 024315 (2002).
[13] N. I. Ashwood *et al*., J. Phys. G **32**, 463 (2006).
[14] M. Freer, Nucl. Instrum. Methods **A383**, 463 (1996).
[15] D. R. Tilley, H. R. Weller, C. M. Cheves, and R. M. Chasteler, Nucl. Phys. **A595**, 1 (1995).
[16] K. P. Artemov *et al*., Yad. Fiz. **37**, 1351 (1983).
[17] D. R. Tilley, C. M. Cheves, J. H. Kelley, S. Ramand, and H. R. Weller, Nucl. Phys. **A636**, 247 (1998).
[18] D. Evers, C. Ley, E. Spindler, W. Assmann, K. Rudolph, P. Konrad, P. Sperr, Nucl. Phys. **A275**, 363 (1977).
[19] K. Gul, B. H. Armitage, and B. W. Hooton, Nucl. Phys. **A153**, 390 (1970).
[20] V. Z. Goldberg, K.-M. Källman, T. Lönroth, P. Manngård, and B. B. Skorodumov, Phys. At. Nucl. **68**, 1079 (2005).
[21] A. Cunsolo, A. Foti, G. Imme, G. Pappalardo, G. Raciti, and N. Saunier, Phys. Rev. C **24**, 476 (1981).
[22] P. Descouvemont and D. Baye, Phys. Rev. C **31**, 2274 (1985).
[23] H. T. Fortune, Phys. Rev. C **18**, 1053 (1978).
[24] A. A. Ogloblin, Phys. Elem. Part. At. Nucl. **3**, 936 (1972).